Resonant and crossover phenomena in a multiband superconductor: Tuning the chemical potential near a band edge

Davide Innocenti,[1] Nicola Poccia,[1] Alessandro Ricci,[1] Antonio Valletta,[2] Sergio Caprara,[1] Andrea Perali,[3] and Antonio Bianconi[1]

[1]*Physics Department, Sapienza University of Rome, Piazzale Aldo Moro 2, 00185 Rome, Italy*

[2]*Institute for Microelectronics and Microsystems, IMM CNR, Via del Fosso del Cavaliere 100, 00133 Roma, Italy*

[3]*School of Pharmacy, Physics Unit, University of Camerino, 62032 Camerino, Italy*

(Received 4 July 2010; revised manuscript received 24 September 2010; published 19 November 2010)

Resonances in the superconducting properties, in a regime of crossover from BCS to mixed Bose-Fermi superconductivity, are investigated in a two-band superconductor where the chemical potential is tuned near the band edge of the second miniband generated by quantum confinement effects. The shape resonances at $T=0$ in the superconducting gaps (belonging to the class of Feshbach-like resonances) is manifested by interference effects in the superconducting gap at the first large Fermi surface when the chemical potential is in the proximity of the band edge of the second miniband. The case of a superlattice of quantum wells is considered and the amplification of the superconducting gaps at the Lifshitz transition of the type neck-collapsing of Fermi surface topology is clearly shown. The results are found to be in good agreement with available experimental data on a superlattice of honeycomb boron layers intercalated by Al and Mg spacer layers.

DOI: 10.1103/PhysRevB.82.184528 PACS number(s): 74.62.−c, 74.70.Ad, 74.78.Fk

I. INTRODUCTION

The main physical properties of the Bardeen-Cooper-Schrieffer—Bose-Einstein crossover (BCS-BEC crossover) at zero temperature for a system of three-dimensional (3D) fermions interacting via a contact pairing interaction can be described with continuity by the BCS (mean-field) equations. Indeed, as shown by Leggett,[1] the ground-state BCS wave function corresponds to an ensemble of overlapping Cooper pairs at weak coupling (BCS regime) and evolves to molecular (non-overlapping) pairs with bosonic character as the pairing strength increases (BEC regime). The crucial point is that the BCS equation for the superconducting gap has to be coupled to the equation that fixes the fermion density: with increasing coupling (or decreasing density), the chemical potential μ results strongly renormalized with respect to the Fermi energy E_F of the non interacting system, and approaches $-\frac{1}{2}E_B$, where E_B is the molecular binding energy of the corresponding two-body problem in the vacuum. In recent years, the experimental realization of the BCS-BEC crossover in trapped ultracold fermion gases allowed for a quantitative test of the validity of increasingly elaborated theoretical approaches: at resonance (the so-called "unitarity limit"), where the lack of a small parameter does not permit the systematic control of the approximations, the BCS theory at zero temperature gives a gap and a chemical potential which are overestimated by about 30% as compared with the results of QMC calculations and the experimental findings, while already the inclusion of pair fluctuations at the (non-self-consistent) t-matrix level improves the comparison for the gap and μ, with deviations not larger than few percents, as shown by quantitative comparison between theoretical predictions and experimental results for the BCS-BEC crossover.[2] The mean field approach at zero temperature, within the local density approximation,[3] or in the form of Bogoliubov–de Gennes equations,[4] has been widely used in the context of ultracold atoms to study nonuniform configurations both in homogeneous space and in the confining potential of the trap, as, e.g., quantized vortices. On the basis of the wide range of quite successful applications discussed above, in this paper we shall apply the BCS approach (with the inclusion of the density equation) to the case of multiband superconductivity with the chemical potential tuned near a band edge. This approach, which has the advantage of being numerically feasible, is also apt to give a good overall insight into the resonant and crossover phenomena which are the object of the present work.

Multigap superconductivity in a system with many minibands of different symmetry has been studied in electronic systems with relevant quantum size effects: single slab,[5,6] single tube,[7] single wire,[8,9] or single quantum dots.[10] The electronic structure generated by the quantum confinement effects gives rise to electron wave functions at the Fermi level near a band edge that are strongly affected by the detail of the quantum confinement. Recently, experimental evidence has been accumulated for superconductivity modulated by quantum confinement effects in a single quantum well and in a single quantum dot.[11–15]

Also superlattices of quantum wires or quantum wells show multiband superconductivity near a band edge.[16–20] The three-dimensional (3D) structure of the superlattice has the advantage to suppress quantum fluctuations, that reduce the critical temperature in low dimensions, while keeping the key features of quantum confinement effects for superconductivity. While there are works on the theory of shape resonances in two-dimensional (2D) superlattices of quantum wires,[21–23] called "superstripes" in cuprate superconductors,[24–26] the theoretical investigation of shape resonances in superlattices of quantum wells is missing. These are now of high interest since a 3D superlattice of quantum wells provide the simplest case of a 3D system showing multiband superconductivity near a band edge. Moreover, it has been recognized that diborides,[27] intercalated graphite,[28–30] and pnictides[31,32] are practical realiza-

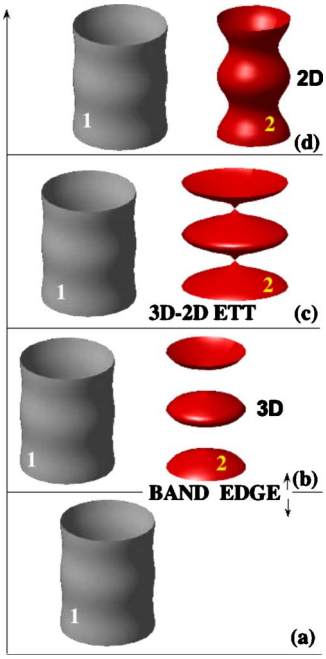

FIG. 1. (Color online) Pictorial view of the evolution of the Fermi surfaces (FS) for the superconductor made of nonhybridized two-bands by moving the chemical potential from panel (a) to panel (d) so that it crosses two Lifshitz electronic topological transitions (ETT). The first ETT occurs moving E_F across the band edge E_{edge} of the second band so that the superconductivity goes from the single FS in panel (a) with a single condensate to the two FS in panel (b) with two condensates: the first (1) has a 2D topology and the second (2) has a 3D topology. Here, ξ is the transversal band dispersion. Changing E_F the system crosses the critical energy $E_{3D\text{-}2D}$ where the second FS undergoes a 3D-2D ETT shown in panel (b) changing its topology: the second closed 3D FS [panel (b)] becomes the tubular 2D FS in panel (d). The first large 2D FS (1) remains nearly constant when the chemical potential is moved.

tions of a superlattice of superconducting layers at atomic limit, where interband pairing is an essential ingredient for high-temperature superconductivity.[16–20]

In this paper, we study the BCS-BEC crossover which occurs in a two-band system, when the chemical potential μ is tuned in a narrow energy range around the edge E_{edge} of the second miniband. This description applies to the situation when the first two minibands produced by quantum size effects in a superlattice of quantum wells are well separated, i.e., when the electron hopping between wells is small enough, to that the corresponding transversal band dispersion ξ is smaller than the energy separation between the minibands.

In Fig. 1 we show that a new 3D Fermi surface (FS) opens when μ is increased above E_{edge}, and the electron gas in the metallic phase undergoes an electronic topological transition (ETT), also called a Lifshitz quantum phase transition, of the type "appearing or disappearing of a new Fermi surface spot."[19,20,33] When μ reaches a higher energy threshold, $E_{3D\text{-}2D}$, the electronic structure of the superlattice undergoes a second ETT, the 3D-2D ETT where one FS changes topology from 3D to 2D (i.e., from "spherical" to "cylindrical") or vice versa, called "the opening or closing of a neck in a tubular FS."[19,20,27,33] This ETT is typical of (i) stacks of metallic layers, (ii) multilayers, or (iii) superlattices of quantum wells, and therefore it is a common feature of all existing high-temperature superconductors and novel materials synthesized by material design in the search for room temperature superconductivity. In practical cases, the tuning of μ at an ETT can be controlled by means of: (i) pressure; (ii) the misfit strain[34–36] between the superconducting layers and the spacers; (iii) the ordering of dopants in the spacers[26] with related striped superstructures; (iv) the effective charge density, via gate voltage methods;[37–39] (v) the charge transfer between the superconducting layers and the spacers; (vi) the thickness of the spacers.

As stated above, we focus on the superconducting properties of a system in which the chemical potential is varied in a narrow energy range around the band edge, within a simple model for a two-band superconductor with a first and a second band of different (even and odd) parity and different topology, which can be varied by tuning the chemical potential. This system provides a particular case of modulated topological multiband superconductor with multiple different winding numbers.[40] We consider the set of coupled BCS equations to study the evolution of the properties of this two-band system of fermions with contact pairing interactions and a pairing energy cutoff ω_0 on the order of magnitude of the distance between μ and the bottom of the second band. Moreover, resonant and crossover phenomena which are the object of this work, are amplified when the transversal dispersion ξ is of the same order of magnitude of ω_0. Therefore, in the following discussion, we concentrate our analysis on systems that are engineered by material science techniques in such a way that $\xi=\omega_0$.

The condensate in the first large 2D FS, in the standard BCS approximation ($E_F/\omega_0 \gg 1$, i.e., E_F far from band edges), coexists with a second small FS, where the standard approximation breaks down [$(E_F-E_{edge})/\omega_0 \ll 1$, i.e., E_F close to the band edge where a new FS disappears or appears, or near the 3D-2D ETT, at the closing or opening of a neck in a tubular FS (Ref. 33)].

When the chemical potential is located near the band edge, it may be driven below the bottom of the conduction band by superconducting correlations, in a way similar to the case of semimetals.[41] The phenomenon of quantum shape resonances[16–20] occurs when the chemical potential falls within an energy range ω_0 near an ETT point. The shape resonances are due to the configuration interaction between paired states in the large FS, with a large group velocity, and quasistationary states near the ETT in the second small FS. The shape resonances in superconducting gaps near an ETT are analogous to the scattering resonances due to configuration interaction between a closed and an open channel described in nuclear physics by Majorana and Feshbach, and in atomic physics by Fano, as reported in a recent work.[42]

In our system, we capture the crucial ingredients of the interplay of the two bands and of the two set of wave functions (which will be shown to be responsible for the shape resonances in the gap and in the critical temperature), without facing the complications beyond BCS theories (as the Eliashberg theory, or corrections beyond Migdal theorem, etc.) which are considered in more conventional (phonon- or

magnon-mediated) strong-coupling superconductors, or the *t*-matrix corrections. These latter would be the dominant corrections in the regime of band-edge crossing, in particular for the evaluation of the critical temperature, but should not qualitatively change our results. Indeed, the Migdal-Eliashberg approach to evaluate the superconducting properties taking into account the frequency dependence of the two-particle interaction (retardation effects) can be applied only when the Fermi energy is much larger than the typical energy of the interaction, i.e., when the Migdal theorem holds. In multiband superconductors, when approaching a band bottom, the two energy scales become comparable and the Migdal theorem cannot be applied (a small parameter controlling the diagrammatic expansion does not exist anymore), requiring the inclusion of much more complicated diagrams, as vertex corrections, in determining the self-consistent equations for the superconducting properties,[43] which is beyond the scope of our work.

We point out that, in this paper, we shall not deal with the problem of superconducting fluctuations in multiband systems, and refer to the different regimes depending on the position of the Fermi energy only. Moreover, we recall that a pure BEC limit with the condensation of pointlike bosons, cannot be achieved when a pairing interaction with a finite energy cutoff is considered in the effective Hamiltonian. When the Fermi energy crosses both the band edge, the condensate in the newly disappearing or appearing FS undergoes a crossover from a mixed Bose-Fermi regime to the BCS regime. Indeed, in the range $-1<(E_F-E_{edge})/\omega_0<0$, the electron states associated with the newly appearing FS are unoccupied in the normal state, and, in the presence of a strong enough pairing interaction, a condensate of boson-like tightly bound pairs[44]is formed below T_c. However, we call this regime the mixed Bose-Fermi regime, because the tightly bound pairs are never genuinely bosonlike, due to the presence of the large band. A preliminary study of the superconducting fluctuations reveal that these have a mixed character, propagating (like in the BEC regime) and damped (like in the BCS regime).

The first unconventional BCS regime occurs in the range $0<(E_F-E_{edge})/\omega_0<1$, where all the few electrons in the newly appearing miniband, condense below T_c. Indeed, in the case under discussion, $\xi=\omega_0$, the standard approximation $(E_F-E_{edge})/\omega_0 \gg 1$ breaks down. In this range, the new appearing FS has a 3D topology while the large FS has a 2D topology.

A second unconventional regime occurs around the 3D-2D ETT where the superconductivity phase in the range $0<(E_F-E_{edge})/\omega_0<2$ arises because of the configuration interaction between pairing channels in different bands with different condensate symmetry 2D and 3D (i.e., with different winding numbers) above and below the 3D-2D ETT.

Finally the system is in the standard multiband BCS regime for $(E_F-E_{edge})/\omega_0>2$.[45–47] There is an analogy between the crossover case studied here and the BEC-BCS crossover in ultracold Fermi gases. While in the ultracold gases the tuning of the energy of the bound state of the diatomic molecule above or below the continuum is performed by using an external magnetic field, here, the ETT in the second narrow miniband can be tuned for example by gate voltage techniques, pressure or misfit-strain, inducing shape resonances in the superconducting properties.

Here, starting from the standard two-band BCS superconductivity in the clean limit[45–47] far from ETT's, we focus on the case when the chemical potential falls within a narrow energy range near a band edge where the Feshbach-like *shape resonance* in superconducting gaps takes place.[19] The shape quantum resonance in the exchangelike interband interactions is generically driven by the repulsive Coulomb interaction and in a two-band model leads to condensate wave functions with opposite signs (a classical quantum phenomenon, recently becoming popular in pnictides with the name of $s\pm$ pairing).[19,20,48,49] We show that the control of the ratio between the intensity of exchangelike interband pairing and intraband Cooper pairing, by material design techniques, is crucial. We discuss the case of different attractive intraband coupling strengths in the first and second miniband and we determine the evolution of the superconducting gaps by changing the interband exchangelike pairing in the crossover regime from the BCS regime, well above the band edge to the mixed Bose-Fermi regime, below the band edge.

We find that the direct evidence for the quantum interference effects between pairing channels is provided by minima in the gap parameter for electrons in the large FS and we show the shift to these minima by changing the interband pairing strength. We report evidence for two different regimes where in the first the interband pairing dominates while in the second the intraband dominates. These regimes are separated by a critical value of the interband pairing where the gap ratio becomes independent on the variation of the chemical potential. Finally, we are able to compare the calculations with the available experimental data for the evolution of the gaps near the band edge of a 2D FS in doped diborides, where intraband dominates, but interband pairing is essential for understanding the evolution of the gaps with the (doping dependent) critical temperature. The comparison with available experimental data for doped diborides in a wide range of doping provides a good test of the present theory.

II. SUPERCONDUCTING GAPS

In a multiband system, near the band edge in the ℓth band, where $\nabla_{\mathbf{k}}E_\ell=0$, the energy of an electron can be approximated by a free-electron dispersion law $E_{\ell,\mathbf{k}}=E_\ell+(\mathbf{k}^2/2m_\ell)$, where m_ℓ is the electron effective mass at the band edge. However, within our model for a superlattice of quantum wells disposed along the z axis, while this approximation is valid to describe the electron dispersion in the x,y plane of the superconducting layers, it is certainly not valid in the z direction, when the transversal band dispersion ξ is on the order of energy cut off of the pairing interaction ω_0. In this case, an anisotropic band with weak dispersion in the z direction and larger dispersion in the x,y plane above the band edge of the second band should be adopted,

$$E_{2,\mathbf{k}}^{3D}=E_{2,L}+E(k_z)+\frac{k_x^2+k_y^2}{2m_\parallel}, \tag{1}$$

where $E(k_z)$ is the actual energy dispersion in the periodic potential of the superlattice and $m_\parallel$ is the effective mass in

the x,y plane. This situation is obtained within a model where a free-electron gas is confined in a potential which is periodic in the z direction,

$$\mathcal{W}(z) = \sum_{n=-\infty}^{n=+\infty} \mathcal{W}_b(z - nd), \tag{2}$$

where $\mathcal{W}_b(z) = -V_b$ for $|z| \leq L/2$ and $\mathcal{W}_b(z) = 0$ for $L/2 < |z| < d/2$, L is the width of the confining well and d is the periodicity of the superlattice in the z direction. This periodic potential mimics the phenomenology, e.g., of the pnictides, diborides, and stacks of graphene layers made of a superlattice of stacked planes. The confining potential generates a band structure organized in minibands. Each miniband has a 3D character, with closed isoenergetic surfaces, near the lower band edge $E_{edge} = E_{\ell,L}$, and a 2D character, with isoenergetic surfaces open in the z direction, above some energy threshold $E_{\text{3D-2D}} = E_{\ell,T}$. The present model is apt to describe quantum interference phenomena between different scattering channels in a large and a small FS which are the object of this work, when μ is tuned near the bottom of a ℓth miniband, within a window of width $4\omega_0$. In the energy window of width $2\omega_0$ the first band, with a large 2D tubular FS, has a constant density of states (DOS) N_1. The second FS disappears (or appears) as E_F crosses the level $E_{edge} = E_{\ell,L}$. The second FS changes from tubular 2D to closed 3D topology as E_F crosses the level $E_{\text{3D-2D}} = E_{\ell,T}$, as it is shown in Fig. 1. Near the edge, the DOS of the second FS, N_2, has the typical 3D behavior shown in Fig. 2(a) in the corresponding range of charge density in the metallic layers between ρ_{edge} and $\rho_{\text{3D-2D}} = \rho_{edge} + \rho_c$.

The crossover from 2D to 3D can be described in our model by changing from an infinite potential barrier between the planes of the superlattice in the z direction, provided by spacer layers, to a finite barrier (V_b). This yields a finite hopping term that broadens the sharp discontinuity of the DOS of a pure 2D band. This broadening increases the width of the shape resonance. Moreover, it is possible to design artificial superlattice heterostructures at optimum shape resonance condition, i.e., where the value of the potential barrier V_b and its width are such that the miniband dispersion in z direction ξ is of the order of energy cutoff ω_0 of the interaction, as we shall assume in the following.

It must be pointed out that, differently from the case of a single 2D slab,[5] in our superlattice,[21] at finite V_b a genuinely 3D condensate is formed, reducing the effect of fluctuations of the superconducting order parameter, which suppress the mean-field value of T_c. Moreover, coexistence of small and large Cooper pairs due to different couplings in the two bands is expected to induce an effective screening of the strong superconducting fluctuations associated with the small pairs.[50]

The pairing interaction is assumed to be originated from an electron-electron contact interaction. Once the matrix elements between exact eigenstates of the superlattice, $\tilde{\mathcal{V}}^{\ell,\ell'}_{\mathbf{k},\mathbf{k}'}$, are calculated they turn out to depend on the wave vector $\mathbf{k}_z$ in the superlattice direction. This induces a structure in the $\mathbf{k}$-dependent interband coupling interaction for the electrons that determines the quantum interference between electron

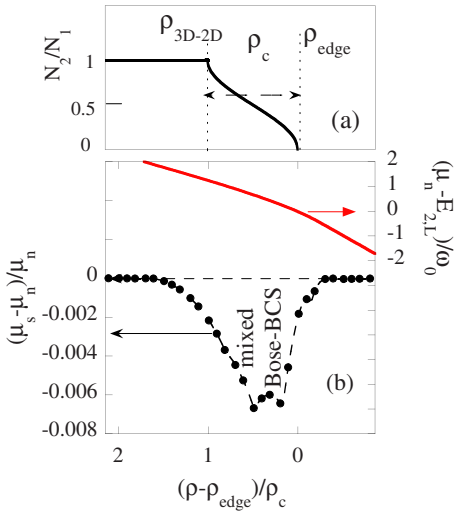

FIG. 2. (Color online) The crossover regime reached by decreasing the charge density in the superlattice from the two-band BCS superconductor to the mixed Bose-Fermi regime at the lover band edge $E_{2,L}$, as a function of the electron charge density $(\rho - \rho_{edge})/\rho_c$, where ρ_{edge} ($\rho_{edge} + \rho_c$) is the charge density where E_F is tuned at E_{edge} ($E_{\text{3D-2D}}$). Panel (a). The ratio of the DOS of the second miniband N_2 and the DOS of the first miniband N_1. Upper part of panel (b): the relative variation of the Lifshitz parameter $(\mu_n - E_{2,L})/\xi$ as a function of electron charge; lower part panel (b): the variation of the chemical potential, $(\mu_s - \mu_n)/\mu_n$, as a function of charge density ρ, where μ_n and μ_s are the chemical potentials in the normal and superconducting phase, $E_{2,L}$ is the lower band-edge energy of the second miniband.

pairs wave functions in different minibands of the superlattice.[19,20] The pairing interaction is then cut off at a characteristic energy ω_0,

$$\mathcal{V}^{\ell,\ell'}_{\mathbf{k},\mathbf{k}'} = \tilde{\mathcal{V}}^{\ell,\ell'}_{\mathbf{k},\mathbf{k}'} \theta(\omega_0 - |\xi_{\ell,\mathbf{k}}|)\theta(\omega_0 - |\xi_{\ell',\mathbf{k}'}|), \tag{3}$$

where $\mathbf{k} = \mathbf{k}_z (\mathbf{k}' = \mathbf{k}'_z)$ is the superlattice wave vector, in the z direction, perpendicular to the planes, of the initial (final) state in the pairing process, and

$$\tilde{\mathcal{V}}^{\ell,\ell'}_{\mathbf{k},\mathbf{k}'} = \frac{c_{\ell,\ell'}}{N_0(E_F) V_{\text{3D}}} I^{\ell,\ell'}_{\mathbf{k},\mathbf{k}'}, \tag{4}$$

where $N_0(E_F)$ is the DOS at E_F for a free-electron 3D system, V_{3D} is the volume of the system,

$$I^{\ell,\ell'}_{\mathbf{k},\mathbf{k}'} = -d \int_d \psi_{\ell,-\mathbf{k}}(z)\psi_{\ell',-\mathbf{k}'}(z)\psi_{\ell,\mathbf{k}}(z)\psi_{\ell',\mathbf{k}'}(z)dz \tag{5}$$

and $\psi_{\ell,\mathbf{k}}(z)$ are the eigenfunctions in the superlattice of quantum wells, normalized so that $\int_d dz |\psi_{\ell,\mathbf{k}}(z)|^2 = 1$. The use of single cutoff in two-band superconductors has been justified in detail by Entel.[51] Here, we assume that pairing in our confined geometry is provided by a contact interaction with a given characteristic energy range. The dimensionless coupling constants $c_{\ell,\ell'} = (2\delta_{\ell,\ell'} - 1)c^0_{\ell,\ell'}$ are positive for $\ell = \ell'$ (intraband Cooper pairing) and negative for $\ell \neq \ell'$ (repulsive exchangelike interband pairing, with $c_{\ell,\ell'} = c_{\ell',\ell}$) and measure the relative intensity of intraband and interband pairing.

Here a comment on the effective interaction adopted in the present work is in order. Our pairing interaction is semiphenomenological in the sense that we do not derive the microscopic expression of the contact pairing interaction (its strength and energy range being used as fitting parameters), but the matrix elements are calculated between eigenstates of the actual confining potential, and in this sense they are microscopic. The choice of ω_0 on the order of the miniband width ξ is justified because this corresponds to the optimum amplification case, as above discussed.

In order to determine the gaps and μ self-consistently at zero temperature we use iterative solving methods for the BCS-like equations

$$\Delta_{\ell,\mathbf{k}} = -\frac{1}{2M}\sum_{\ell',\mathbf{k}'} \frac{\mathcal{V}^{\ell,\ell'}_{\mathbf{k},\mathbf{k}'}\Delta_{\ell',\mathbf{k}'}}{\sqrt{(E_{\ell',\mathbf{k}'}-\mu)^2+\Delta^2_{\ell',\mathbf{k}'}}}, \tag{6}$$

$$\rho = \frac{1}{Md^2}\sum_{\ell,\mathbf{k}}\left[1-\frac{E_{\ell,\mathbf{k}}-\mu}{\sqrt{(E_{\ell,\mathbf{k}}-\mu)^2+\Delta^2_{\ell,\mathbf{k}}}}\right], \tag{7}$$

where M is the total number of wave vectors $\mathbf{k}'$ and ρ is the electron density, starting with initial constant gaps and an initial μ equal to the value of E_F in the normal state. We considering convergence to have occurred when the relative variation of the gap and charge density ρ less than 10^{-6}. We point out that the gap functions $\Delta_{\ell,\mathbf{k}}$ depend on the superlattice wave vector $\mathbf{k}$ as well as on the miniband index ℓ. The BCS-like equations self-consistently couple the gap function at a given point of $\mathbf{k}$-space with the values of the gap function in the entire $\mathbf{k}$-space. In the following we discuss the properties of the average values of the gap in $\mathbf{k}$-space, unless otherwise specified. The above equations can be easily generalized to finite temperatures T, but in the remaining part of the present section we focus on the case $T=0$.

In the standard BCS theory, where E_F is far from the band edges, the relative variation of μ going from the normal to the superconducting state is expected to be negligible. This is not true when μ is tuned near the band edge of the second band. In fact, our calculation yields a significant variation of μ in the superconducting phase, as a function of the charge density [Fig. 2(b)]. A relative variation of μ going from the normal to the superconducting phase, as large as 10^{-3}, is obtained near the band edge and at the 3D-2D ETT, within a range $4\omega_0$. The variation starts to be large, as compared with the standard BCS result, in proximity of the crossover regime below the band edge up to well beyond the 3D-2D ETT.

The Feshbach-like shape resonance regime occurs in correspondence of the large variation of μ between the normal and superconducting phases shown in Fig. 2(b). In Fig. 3 we report the distribution of values of the matrix elements $I^{\ell,\ell'}_{\mathbf{k},\mathbf{k}'}$ in the first two minibands, for the case with miniband dispersion $\xi=\omega_0$. The intraband distributions of the two bands show different shapes and widths and have different range of values. The resulting matrix of coupling constants is obtained exclusively from the eigenfunctions of the superlattice and is noticeably asymmetric.

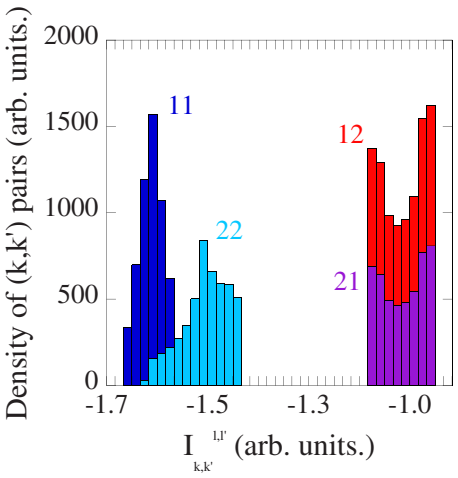

FIG. 3. (Color online) Density histograms of the pairing interaction matrix elements $I^{\ell,\ell'}_{\mathbf{k},\mathbf{k}'}$ between the first and the second minibands, for the case with miniband dispersion $\xi=\omega_0$. Histograms 11, 22, 21, and 12, shows, respectively, the pairing interaction matrix elements $I^{1,1}_{\mathbf{k},\mathbf{k}'}$, $I^{2,2}_{\mathbf{k},\mathbf{k}'}$, $I^{2,1}_{\mathbf{k},\mathbf{k}'}$, and $I^{1,2}_{\mathbf{k},\mathbf{k}'}$.

The gap parameters in the two bands have a sizable dependence on the wave vector k_z as shown in Fig. 4 for the gap in the first miniband, taking the average value of the gap over the wave vectors as a reference value. The wave-vector dependence of the gaps is induced by the effective interaction $V^{\ell,\ell'}_{\mathbf{k},\mathbf{k}'}$ entering the BCS equations, which by itself has a nontrivial dependence on the wave vectors of the two scattered electrons forming the Cooper pairs, as discussed above. The largest values of the gaps are found in our calculations for large transversal wave vectors, suggesting that the effective pairing interaction is mostly affected by the superlattice at small distances of the order of the modulation of the confining periodic potential. Therefore, all the superconducting properties (coherence length, critical temperature, gaps to T_c ratios) are expected to be influenced by superlattice effects

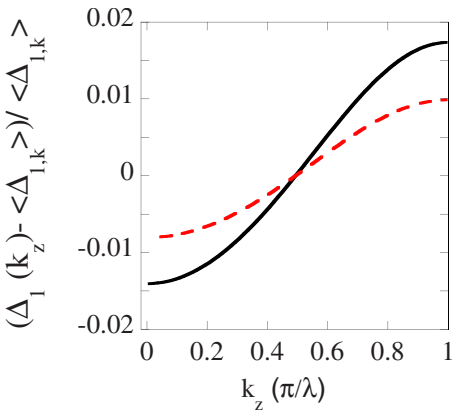

FIG. 4. (Color online) Calculation of the gap anisotropy, i.e., the dependence of the gap in the first miniband, with $c_{22}/c_{11}=2.17$, $c_{11}=0.22$ and $c_{12}/c_{11}=0.43$ as function of the wave vector k_z in the transversal direction. We show in the figure two characteristics cases with different values of the averaged gap obtained solving the BCS-like equations at finite temperatures $T=5.7$ K (solid line) and $T=27.2$ K (dashed line) in the first miniband.

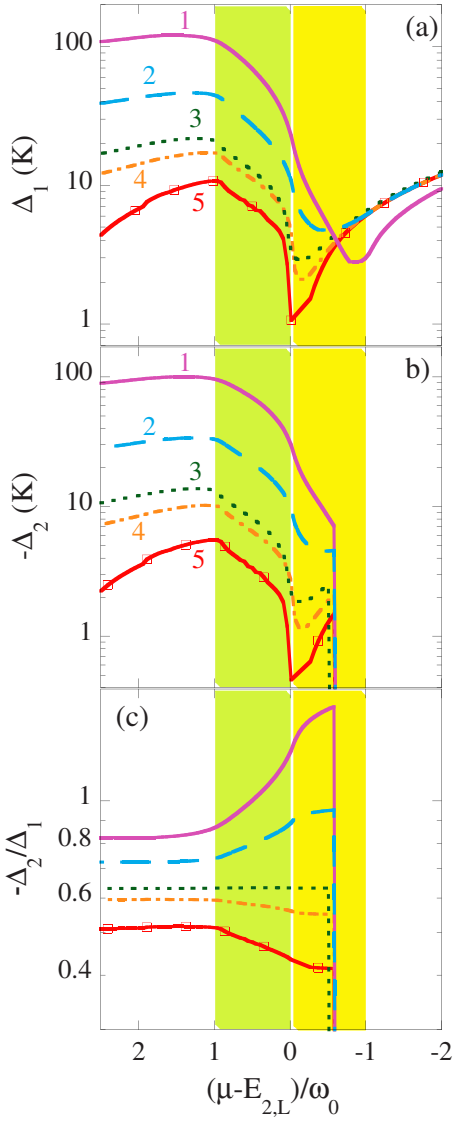

FIG. 5. (Color online) The evolution of the gap, averaged in the k_z direction, in the first miniband [panel (a)] and in the second one [panel (b)] as a function of the Lifshitz parameter, with $c_{22}/c_{11}=0.45$ and $c_{11}=0.22$. The ratio of the gaps as a function of the Lifshitz parameter is reported in panel (c). Several interband coupling ratio cases are reported: curve 1 (solid line) shows the case for $c_{12}/c_{11}=-2.73$, curve 2 (dashed line) shows the case for $c_{12}/c_{11}=-1.59$, curve 3 (dotted line) shows the case for $c_{12}/c_{11}=-1.04$, curve 4 (dot-dashed line) shows the case for $c_{12}/c_{11}=-0.91$ and curve 5 (solid line with open squares) shows the case for $c_{12}/c_{11}=-0.68$. The curve 3 (dotted line) shows the critical case of interband pairing $-c_{12}^{critical}=\sqrt{c_{11}c_{22}}/0.656$ where the gap ratio remains constant going from the two-gap BCS Fermi case to the mixed Bose-Fermi regime at the band edge.

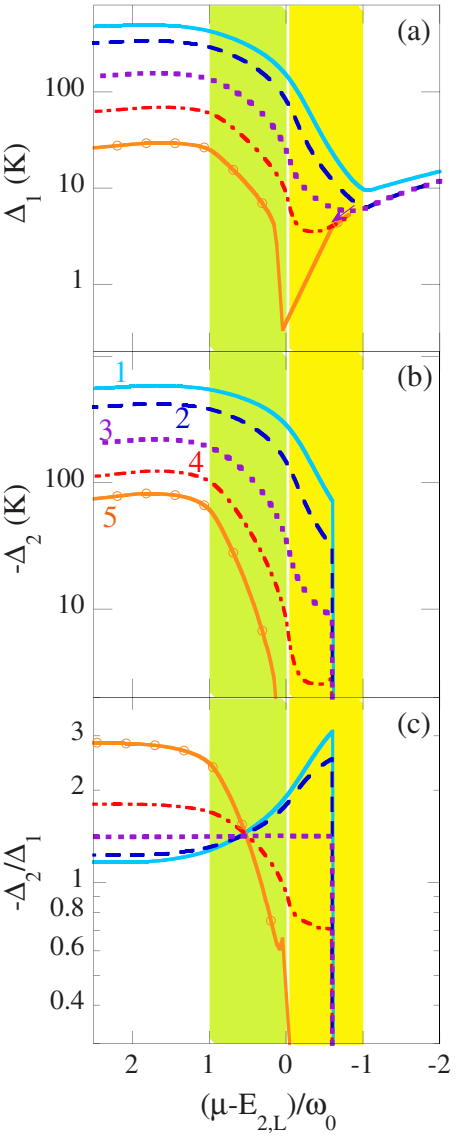

FIG. 6. (Color online) The evolution of the gap, averaged in the k_z direction, in the first miniband [panel (a)] and in the second one [panel (b)] as a function of the Lifshitz parameter, with $c_{22}/c_{11}=2.17$ and $c_{11}=0.22$. The ratio of the gaps as a function of the Lifshitz parameter is reported in panel (c). Several interband coupling ratio cases are reported: curve 1 (solid line) shows the case for $c_{12}/c_{11}=-6.09$, curve 2 (dashed line) shows the case for $c_{12}/c_{11}=-4.34$, curve 3 (dotted line) shows the case for $c_{12}/c_{11}=-2.24$, curve 4 (dot-dashed line) shows the case for $c_{12}/c_{11}=-1.08$ and curve 5 (solid line with open squares) shows the case for $c_{12}/c_{11}=-0.43$. The curve 3 (dotted line) shows the critical case of interband pairing $-c_{12}^{critical}=\sqrt{c_{11}c_{22}}/0.656$ where the gap ratio remains constant from the two-gap BCS Fermi case to the mixed Bose-Fermi regime at the band edge.

via the wave vector dependence of the gap parameters in different bands.

The variation of the gaps at $T=0$ as function of the chemical potential in different coupling regimes is plotted in Figs. 5 and 6. In both figures, the average value of the two gaps taken over the transversal wave vector k_z is reported. In Fig. 5 we consider the case where the intraband coupling in the second miniband is *smaller* than the intraband coupling in the first miniband, i.e., $c_{22}/c_{11}=0.45$. In particular, we report the gaps in the first [panel (a)] and second [panel (b)] miniband as a function of the chemical potential tuned in the vicinity of the bottom of the second miniband. The ratio between the two gaps is reported in the same figure, panel (c). Several interband couplings are considered, spanning from ($c_{12}=c_{21}=-0.15$) to ($c_{12}=c_{21}=-0.60$). Interestingly, a

pronounced minimum is present for the average value of the gap at the FS of the first miniband, Δ_1, when the chemical potential approaches the bottom of the second miniband from below. The partial DOS and the intraband coupling in the first miniband do not change moving the chemical potential therefore the presence of a pronounced minimum supports the existence of antiresonances in the superconducting gaps induced by the interplay between the wave vector and band index dependence of the effective interaction (in which the superposition of single-particle wave functions gives rise to interference effects). The depth of the minimum and its energy position depend on the interband exchangelike pairing. It generally appears below the band edge, where the DOS of the second miniband changes abruptly. It occurs well below the band edge for strong interband pairing and moves toward the band edge by decreasing the interband pairing. The details of the antiresonance depend on the interband coupling, but its presence is a robust feature.

The average value of the superconducting gap at the FS of the second miniband, Δ_2, appears below the energy of the band edge where the chemical potential enters in the second miniband. It displays a strong interband coupling dependence [see Fig. 5, panel (b)]. The ratio $-\Delta_2/\Delta_1$ reaches a constant energy independent value at a critical value $c_{12}^{critical}$ of the repulsive exchangelike interband pairing. The average value of the superconducting gap at the FS of the second miniband, Δ_2, shows an antiresonance minimum for $|c_{12}| < |c_{12}^{critical}|$. The gap ratio $-\Delta_2/\Delta_1$ shows a divergent enhancement moving the chemical potential from the two-gap BCS regime well above the band edge toward the mixed Bose-Fermi regime near the edge for $|c_{12}| > |c_{12}^{critical}|$. The gap ratio $-\Delta_2/\Delta_1$ decreases moving the chemical potential from the two-gap BCS regime well above the band edge toward the mixed Bose-Fermi regime reaching a minimum at the band edge and increasing below the band edge for $|c_{12}| < |c_{12}^{critical}|$, as shown in Fig. 5, panel (c). When the chemical potential is well inside the second miniband, the two gaps recover the standard behavior of a two-band superconductor, with the gap ratio related to the coupling ratio c_{22}/c_{11}. Therefore $-\Delta_2/\Delta_1$ remains smaller than one in the present case. The results show clearly that in the crossover regime there is a critical interband pairing $c_{12}^{critical}$ that separates a first regime of strong interband, where the gap ratio $-\Delta_2/\Delta_1$ increases with moving the chemical potential toward the band edge from a second regime of weak interband, where the gap ratio $-\Delta_2/\Delta_1$ decreases approaching the band edge.

In Fig. 6 we consider the case where the intraband coupling in the second miniband is *larger* than the intraband coupling in the first miniband, i.e., $c_{22}/c_{11}=2.17$. In particular, the gaps in the first [panel (a)] and second [panel (b)] miniband as a function of the chemical potential tuned at the bottom of the second miniband are reported, together with the ratio between the two gaps in panel (c). The calculations have been carried out for several interband couplings, spanning from weak ($c_{12}=c_{21}=-0.51$) to strong interband exchangelike repulsive coupling (=−1.4). The pronounced antiresonance minimum is clearly present for Δ_1. The ratio $-\Delta_2/\Delta_1$ reported in panel (c) of Fig. 6 reaches a constant energy independent value at the critical value $c_{12}^{critical}$ of the repulsive exchangelike interband pairing.

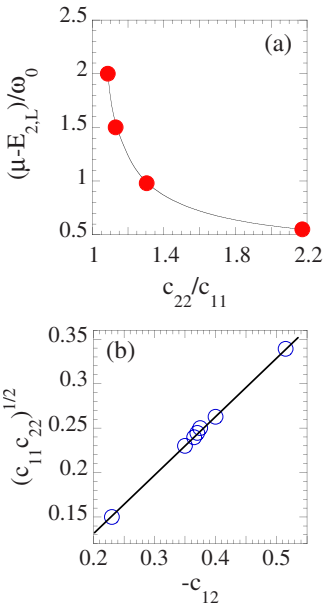

FIG. 7. (Color online) Panel (a): the variation of the critical chemical potential (solid line with filled circles) as a function of intraband coupling ratio c_{22}/c_{11}. We observe that for the intraband coupling ratio approaching unity the critical chemical potential goes to infinity. Panel (b): the variation of the critical interband pairing as a function of $\sqrt{c_{11}c_{22}}$. We observe a linear fit $\sqrt{c_{11}c_{22}} = -0.656c_{12}^{critical}$ (solid line) of calculated $c_{12}^{critical}$ points for the cases of $\sqrt{c_{11}c_{22}}$ (open circles) that divide the plane space in two regions: the upper one, for $\sqrt{c_{11}c_{22}} > -c_{12}^{critical}$, in weak interband regime, where $\partial(-\Delta_2/\Delta_1)/\partial\mu > 0$ and the lower one, for $\sqrt{c_{11}c_{22}} < -c_{12}^{critical}$, in strong interband regime, where $\partial(-\Delta_2/\Delta_1)/\partial\mu < 0$.

Our results for the case $c_{22}/c_{11} > 1$ show that the ratio $-\Delta_2/\Delta_1$ display another relevant feature: at a critical position of the chemical potential the ratio between the two gaps becomes universal, i.e., independent of the value of the interband coupling. The critical chemical potential in Fig. 6 is above the bottom of the second miniband, at a distance about $\frac{1}{2}\omega_0$ from it. This is again a signature of interference effects in the effective pairing, resulting in a fixed point between an antiresonance and a resonance in the superconducting gaps. In Fig. 6 we observe that well above the band edge, in the standard two-gap BCS regime, the gap ratio $-\Delta_2/\Delta_1$ is larger than one, when such is the ratio between the intraband couplings. Increasing the interband pairing we observe that there is a value of the chemical potential at which there is a reversal of the ratio $-\Delta_2/\Delta_1$.

The critical point of the chemical potential where the gap ratio is independent of the interband pairing for $c_{22}/c_{11} > 1$ depends on the ratio between the intraband attractive couplings in the two bands. The variation of the critical chemical potential, present only for the case $c_{22} > c_{11}$, depends on the ratio between the intraband couplings $c_{22}/c_{11} > 1$, as it is shown in Fig. 7 [panel (a), dashed blue line]. The critical chemical potential goes to infinity when the couplings are equal and decreases toward the band edge with increasing the ratio between the coupling in the second band on the coupling in the first band. The critical interband pairing $c_{12}^{critical}$ increases linearly with increasing $\sqrt{c_{11}c_{22}}$, as it is

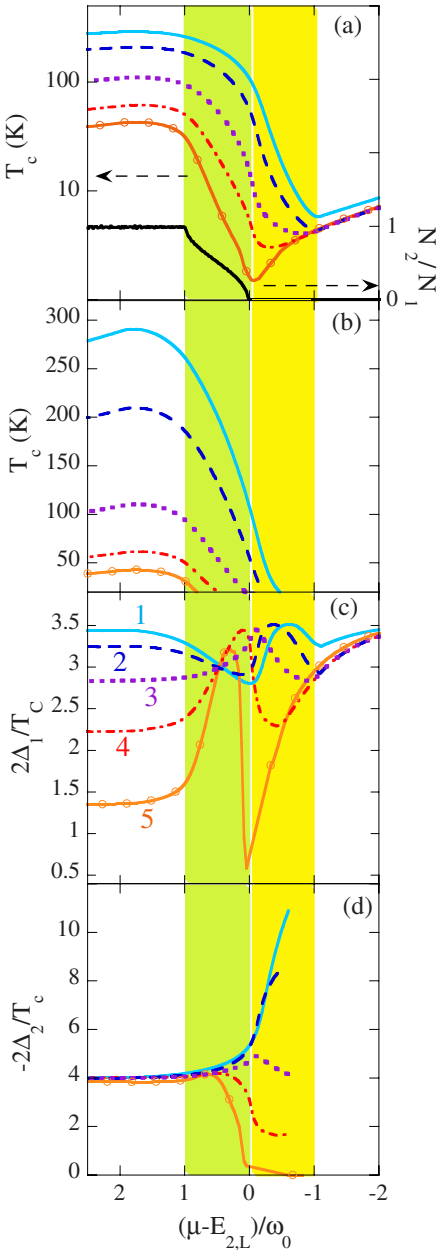

FIG. 8. (Color online) The case of strong coupling in the second band (the so-called diboride case) with $c_{22}/c_{11}=2.17$ and $c_{11}=0.22$. The variable ratio $u=N_2/N_1$ (solid black line) is shown in panel (a). The critical temperature T_c [panels (a) and (b)], the ratio $2\Delta_1/T_c$ [panel (c)], the ratio $-2\Delta_2/T_c$ [panel (d)], as functions of the reduced Lifshitz parameter $(\mu-E_{2,L})/\omega_0$. Several values of the interband coupling ratio are reported: curve 1 (solid line) shows the case for $c_{12}/c_{11}=-6.09$, curve 2 (dashed line) shows the case for $c_{12}/c_{11}=-4.34$, curve 3 (dotted line) shows the case for $c_{12}/c_{11}=-2.24$, curve 4 (dot-dashed line) shows the case for $c_{12}/c_{11}=-1.08$ and curve 5 (solid line with open squares) shows the case for $c_{12}/c_{11}=-0.43$. For the largest value of c_{12} considered here, the critical temperature reaches 300 K, in the range $1<(\mu-E_{2,L})/\omega_0<2$. At the antiresonance for $(\mu-E_{2,L})/\omega_0=0$, T_c and $2\Delta_1/T_c$ reach the minimum value for weak interband interaction. On the contrary, for large interband interaction, $2\Delta_1/T_c$ and T_c reach the minimum value at $(\mu-E_{2,L})/\omega_0=-1$, where T_c reaches room temperature for the chosen set of parameters.

shown in Fig. 7 [panel (b), solid red line]. The data can be fitted with the linear relation $\sqrt{c_{11}c_{22}}=-0.656c_{12}^{critical}$, as it is shown in Fig. 7 [panel (b)].

III. CRITICAL TEMPERATURE

The superconducting critical temperature T_c is calculated by iteratively solving the linearized gap equation,

$$\Delta_{\ell,\mathbf{k}}=-\frac{1}{2M}\sum_{\ell',\mathbf{k}'}\mathcal{V}_{\mathbf{k},\mathbf{k}'}^{\ell,\ell'}\frac{\tanh\left(\frac{\xi_{\ell',\mathbf{k}'}}{2T_c}\right)}{\xi_{\ell',\mathbf{k}'}}\Delta_{\ell',\mathbf{k}'}, \tag{8}$$

until the nontrivial solution (having eigenvalue 1) is reached with increasing temperature.

Below, we present numerical results for the solution of the self-consistent linearized BCS equations which determines the value of the critical temperature and of the chemical potential. We analyze the behavior of the ratios $2\Delta_1/T_c$ and $2\Delta_2/T_c$, where, according to our notation, Δ_1 and Δ_2 are the average values of the wave-vector dependent gaps on the corresponding branches of the FS at $T=0$. Note that the gaps to T_c ratios are physical quantities which are very suitable for quantitative comparison with experiments. Indeed, gaps at $T=0$ (or temperature below $0.4T_c$ in real experimental conditions), and T_c can be extracted in a single experimental run when measuring the temperature dependence of the superconducting gaps in multiband superconductors.

We focus here on the case characterized by a coupling in the second FS larger than in the first FS. As an example of this regime, we calculate the DOS for the second miniband, T_c, $2\Delta_1/T_c$, and $-2\Delta_2/T_c$ as functions of the reduced Lifshitz parameter $(\mu-E_{2,L})/\omega_0$, with intraband coupling terms fixed to $c_{11}=0.23$, $c_{22}/c_{11}=2.17$, for several values of the interband coupling ratio, as shown in the panels (a-d) of Fig. 8.

The minima of T_c, due to the *shape antiresonances*, are all below the band-edge energy of the second miniband [panel (a)] while the maximum value of T_c, due to the *shape resonance*, is reached near the 3D-2D ETT of the second miniband, on its 2D side [panel (b)]. We observe that the *shape resonances* in the gap to T_c ratios show clear evidence for the typical asymmetric line shape of Fano-Feshbach quantum resonances driven by configuration interaction between different scattering channels. The antiresonance due to negative interference effects appears in the range between $(\mu-E_{2,L})/\omega_0=-1$ and $(\mu-E_{2,L})/\omega_0=0$, where T_c has a minimum in panel (a) followed by the T_c resonance maximum in the range $(\mu-E_{2,L})/\omega_0=1.5$.

For strong exchangelike interband pairing, $c_{12}>c_{12}^{critical}$, we find that the ratio $2\Delta_1/T_c$ shows two minima and the ratio $2\Delta_2/T_c$ shows an increasing divergence in the mixed Bose-Fermi regime. Decreasing the interband pairing, for $c_{12}<c_{12}^{critical}$, the minimum due to the negative interference effect in $2\Delta_1/T_c$ at $(\mu-E_{edge})/\omega_0=-1$, associated with the Feshbach-like *shape resonance* at the band edge, moves toward $(\mu-E_{edge})/\omega_0=0$. The ratio $2\Delta_1/T_c$ shows a maximum at $(\mu-E_{edge})/\omega_0=0$ [dotted line in panel (c) of Fig. 8] for the critical value of the interband pairing, $c_{12}^{critical}$.

IV. CASE OF THE SUPERLATTICE OF ATOMIC BORON LAYERS: DOPED MgB_2

The present shape resonance superconductivity scenario in a multiband superconductor tuning the chemical potential near a band edge can be tested in the particular experimental case of doped magnesium diboride. Doped MgB_2 is a practical realization of a heterostructure at atomic limit[16] being made of first units, superconducting atomic boron layers (similar to graphene layers), intercalated with second units (playing the role of spacers), hexagonal Mg layers, forming a superlattice of quantum wells with a period of 0.35 nm.[27,52] The electronic structure near the Fermi level resulting from the material architecture is made of a first large Fermi surface (π-band) and second small Fermi surface (σ-band) with different symmetry and spatial locations. The DOS at the Fermi energy in MgB_2 is 0.12 states/(eV atom spin), where about one half (exactly 44%) of this value comes from the σ-bonds and the other half (exactly 56%) comes from the π-bonds. The chemical potential E_F in MgB_2 is separated by about 700 meV from the band edge energy at the top E_Γ of the σ-band and it is separated by about 300 meV from the energy of the 3D-2D ETT at the E_A point in the band structure.

The chemical potential can be tuned near the band edge of the sigma band (at the critical point $E_{edge}=E_\Gamma$ in the band structure) and across the 3D-2D ETT (at the critical point $E_{3D\text{-}2D}=E_A$ in the band structure) by chemical substitution of Al (Refs. 27 and 53–55) and Sc (Ref. 56) for Mg or C for B.[57,58] The different superconducting gaps in both bands and the critical temperature have been measured as a function of the chemical potential across the 3D-2D ETT by several groups in Al doped samples,[59–63] and in carbon doped samples.[64] The physical properties around the 3D-2D ETT are plotted here for the case of doped MgB_2 as a function of the reduced Lifshitz parameter "z"$=(E_\Gamma-E_F)/(E_A-E_\Gamma)$, where $\xi_0=E_A-E_\Gamma$ is the energy dispersion in the c-axis direction due to electron hopping between the boron layers (400 meV in MgB_2 and it changes with chemical substitution x). The influence of the proximity to an ETT (Ref. 65) on the anomalous electronic and lattice properties of MgB_2 is shown by the anomalous pressure dependence[66] and Raman lineshape[67] of the E_{2g} phonon mode.

The multiband superconducting phase of MgB_2 in the clean limit has been studied theoretically in detail[47,68–70] and its properties have been extracted from experimental data.[64,71] The ratio between the intraband electron-phonon (p-h) coupling in the σ-band, c_{22}, and in the π-band, c_{11}, is in the range $2<c_{22}/c_{11}<2.6$ and the ratios between the interband coupling constant and the intraband coupling constants are $0.15<c_{12}/c_{22}<0.3$ and $0.4<c_{12}/c_{11}<1$. The system is therefore in the regime of strong coupling in the second band and weak interband coupling discussed above. The interband coupling is smaller than the critical interband coupling $-c_{12}^{critical}=\sqrt{c_{11}c_{22}}/0.656$: from the published data we find $0.2<c_{12}/(-c_{12}^{critical})<0.5$. Therefore the shape resonance regime for the doped MgB_2 system is well described by the typical case in Fig. 6 shown as the curve 5 where $c_{22}/c_{11}=2.17$, $c_{12}/c_{11}=-0.43$ and $c_{12}/(-c_{12}^{critical})=0.19$. For diborides there is a lack of a focused experimental test for the so-called $s\pm$ pairing, driven by the repulsive Coulomb interaction in the two band superconductivity with negative interband coupling. This will lead to condensate wave functions with opposite signs as it is proposed here. Therefore we hope that an experiment like for pnictides[48] will be run in the near future. However the critical temperature and the absolute values of the gaps calculated here does not depend in the sign of the interband coupling. The critical temperature (panel a) superconducting gaps (panel b) in doped MgB_2 are

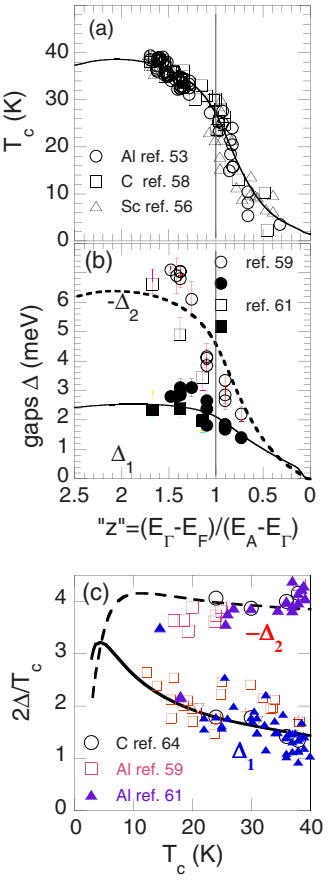

FIG. 9. (Color online) Panel (a): The superconducting critical temperature in Al for Mg substitution $(Mg_{1-x}Al_x)B_2$, (open circles),[53] in Sc for Mg substitution $(Mg_{1-x}Sc_x)B_2$,(open triangles)[56] and for the C for B substitution in the $Mg(C_xB_{1-x})_2$ system (open squares)[58] as function of the Lifshitz parameter "z"$=(E_\Gamma-E_F)/(E_A-E_\Gamma)$ for diborides.[53,56,58] Panel (b). The gaps $\Delta_1=\Delta_\sigma$ (open symbols) and $\Delta_2=\Delta_\pi$ (filled symbols) in Al for Mg substitution $(Mg_{1-x}Al_x)B_2$,[59] and for the C for B substitution in the$Mg(C_xB_{1-x})_2$ system[64] as function of the Lifshitz parameter "z"$=(E_\Gamma-E_F)/(E_A-E_\Gamma)$ calculated for aluminum[53,54] and carbon[57] substitutions based on theoretical calculations and structural data. Panel (c). The BCS ratios curves $2\Delta_1/T_c$ (solid line) and $-2\Delta_2/T_c$ (dashed line), as functions of T_c, extracted from the experiments measuring in the same run the two gaps well below the critical temperature and T_c.[59–63] Carbon doped samples,[64] (open circles). Al doped samples from Daghero *et al.*[59] (open squares), and from Samuely *et al.*[61] (triangles). The experimental data are compared with the calculated curves in the case $c_{22}/c_{11}=2.17$, $c_{12}/c_{11}=-0.43$, where $-c_{12}=0.10$ is lower than the value $(-c_{12}^{critical})=0.52$, where the critical temperature, and the gaps are calculated as a function of $(\mu-E_{2,L})/\xi_0$.

shown in Fig. 9 as a function of the Lifshitz parameter "z." The Lifshitz parameter "z" has been calculated at each chemical doping value x in the case of the Al substitution for Mg $(Mg_{1-x}Al_x)B_2$,[53–55] for the case of Sc substitution for Mg in the $(Mg_{1-x}Sc_x)B_2$ system[56] and for the C for B substitution in the $Mg(C_xB_{1-x})_2$ system[57,58] based on the measured variation of the lattice parameters and the charge density using band structure calculations.[53–55,57] Figure 9(a) shows the universal scaling of the critical temperature T_c, as a function of the Lifshitz parameter "z" while the doping mechanism is quite different for the aluminum,[53,54] scandium,[56] and carbon[57,58] chemical substitutions in diborides. It is clear that the critical temperature curves collapse on the same curve for all cases when they are plotted as a function of "z." The experimental data are plotted in the same figure with the theoretical calculations for the generic T_c and gaps behavior for the case 5 in Fig. 6 and it is possible to appreciate the good agreement between theory and experimental data. In Fig. 9(c), the BCS gap ratios $2\Delta_1/T_c$ and $-2\Delta_2/T_c$ of aluminum doped and carbon doped diborides are plotted as functions of T_c and are compared with the same theoretical case discussed above. The agreement between our theoretical calculations and the available experimental data is satisfactory for the dependence of T_c, the gaps, and the BCS ratio in a wide range of aluminum doping of magnesium diborides. The difference between the experimental data and the present calculations is related with the fact the intraband coupling in the second band is likely to depend on the chemical potential,[67] whereas we assume it to be constant, to reduce the number of parameters. Further work is under progress for a quantitative investigation of shape resonances in doped diborides. These results show clearly that superconductivity in doped diboride superlattices remain in the clean limit for interband pairing although the large number density of impurity centers in doped samples and the structural phase separation.[67] Indeed, it has been pointed out that the shape resonance mechanism can be favored by phase separation and especially for fractal distributions in superstripes.[21–23]

V. CONCLUSIONS

The theoretical analysis discussed in this paper was motivated by the crucial observation that interband pairing may yield a sizable enhancement of the critical temperature in multiband materials, displaying superconductivity in the clean limit, possibly leading to room temperature superconductivity,[16] and is the first step toward the understanding of the role of *shape resonances* in the superconducting gaps in multilayer systems. Although limited to the BCS mean-field approximation, our approach captures the main ingredients of the physics of these systems. In particular, once the relevant details of the wave functions and of the band dispersions of the multilayer structure are introduced in the coupled BCS-like equations for the gaps in the various bands and for the conservation of the electron density, the resonance physics can be investigated in the very same spirit of the BCS-BEC crossover in fermion gases, where a similar approach proved to be predictive.

In real materials, the shape resonances can be controlled with material science techniques, tuning the pairing strength and tailoring the thickness of the spacer layers, to adjust the electron hopping between superconducting layers. In our theoretical approach, the crucial parameter to take into account the effects of hopping variations on the characteristics of the shape resonance, is the dispersion ξ. Resonance effects are emphasized when ξ is on the order of the energy cutoff ω_0 of the effective pairing interaction leading to Cooper pairing. In this paper, we devoted our analysis to the case $\xi=\omega_0$, but of course ξ can be varied around the optimal amplification value, and an analysis of the dependence of resonance effects on the value of ξ will be the object of future investigation.

The main outcomes of our theoretical scenario for superconducting multilayers or multigap superconductors have been tested here on aluminum-doped magnesium diboride superconductors. The quantitative comparison between our theoretical results and available experimental data for this material is satisfactory and permits to identify, e.g., the relevant range of values for the pairing coupling constants.

Our approach can be easily extended to pursue a preliminary investigation of the superconducting properties of other multiband system where the chemical potential is tuned near a ETT in one of the bands. For instance, it could be applied to Fe-based 1111, 122, and 11 pnictides.

On the basis of our analysis, we may start to indicate a possible roadmap for the discovery of novel HTS.[16] The conditions for higher temperature superconductivity, or even room temperature superconductivity, might be met in graphene superlattices[72] where the exchange-like interband interaction could be even stronger than the intraband Cooper pairing, as also predicted for superlattices of carbon nanotubes.[22]

ACKNOWLEDGMENTS

We thank Rocchina Caivano, and Valeria D'Andrea for help in the early stage of this work. We are grateful to Arkady A. Shanenko and I. Eremin for useful discussions.

[1] A. J. Leggett, *Modern Trends in the Theory of Condensed Matter*, edited by A. Pekalski and R. Przystawa, Lecture Notes in Physics (Springer-Verlag, Berlin, 1980), Vol. 115, p. 13.

[2] A. Perali, P. Pieri, and G. C. Strinati, Phys. Rev. Lett. **93**, 100404 (2004) and references therein.

[3] A. Perali, P. Pieri, and G. C. Strinati, Phys. Rev. A **68**, 031601 (2003).

[4] S. Giorgini, L. P. Pitaevskii, and S. Stringari, Rev. Mod. Phys. **80**, 1215 (2008) and reference therein.

[5] J. M. Blatt and C. J. Thompson, Phys. Rev. Lett. **10**, 332 (1963).

[6] A. A. Shanenko, M. D. Croitoru, and F. M. Peeters, EPL **76**, 498 (2006).

[7] C. Thompson, J. Phys. Chem. Solids **26**, 1053 (1965).
[8] A. Perali, A. Bianconi, A. Lanzara, and N. L. Saini, Solid State Commun. **100**, 181 (1996).
[9] A. A. Shanenko and M. D. Croitoru, Phys. Rev. B **73**, 012510 (2006).
[10] V. Z. Kresin and Y. N. Ovchinnikov, Phys. Rev. B **74**, 024514 (2006).
[11] Y. Guo *et al.*, Science **306**, 1915 (2004).
[12] S. Bose, P. Raychaudhuri, R. Banerjee, P. Vasa, and P. Ayyub, Phys. Rev. Lett. **95**, 147003 (2005).
[13] Y. F. Zhang, J. F. Jia, T. Z. Han, Z. Tang, Q. T. Shen, Y. Guo, Z. Q. Qiu, and Q. K. Xue, Phys. Rev. Lett. **95**, 096802 (2005).
[14] C. Brun, I. P. Hong, F. Patthey, Yu R. Heid, P. M. Echenique, K. P. Bohnen, E. V. Chulkov, and W. D. Schneider, Phys. Rev. Lett. **102**, 207002 (2009).
[15] S. Bose, A. M. Garcia-Garcia, M. M. Ugeda, J. D. Urbina, C. H. Michaelis, I. Brihuega, and K. Kern, Nature Mater **9**, 550 (2010).
[16] A. Bianconi, U.S. Patent of the U.S. Patent and Trademark Office (PTO), No. 6,265,019 (4 July, 2001).
[17] A. Bianconi and M. Missori, J. Phys. I **4**, 361 (1994).
[18] A. Bianconi, Solid State Commun. **89**, 933 (1994).
[19] A. Bianconi, J. Supercond. Novel Magn. **18**, 25 (2005).
[20] A. Bianconi and M. Filippi, in *Symmetry and Heterogeneity in high temperature superconductors*, edited by A. Bianconi, Nato Science Series II Mathematics, Physics and Chemistry Vol. 214 (Springer, Dordrecht, 2006), pp. 21–53.
[21] A. Bianconi, A. Valletta, A. Perali, and N. L. Saini, Physica C **296**, 269 (1998).
[22] A. Bianconi, Phys. Status Solidi A **203**, 2950 (2006).
[23] R. Caivano, M. Fratini, N. Poccia, A. Ricci, A. Puri, Z.-A. Ren, X.-L. Dong, J. Yang, W. Lu, Z.-X. Zhao, L. Barba, and A. Bianconi, Supercond. Sci. Technol. **22**, 014004 (2009).
[24] A. Bianconi, N. L. Saini, S. Agrestini, D. Di Castro, and G. Bianconi, Int. J. Mod. Phys. B **14**, 3342 (2000).
[25] A. Bianconi, D. Di Castro, N. L. Saini, and G. Bianconi, in *Phase Transitions and Self-Organization in Electronic and Molecular Networks*, edited by M. F. Thorpe and J. C. Phillips, Fundamental Materials Research (Kluwer Academic Publishers, Boston, 2002), Chap. 24, pp. 375–388.
[26] M. Fratini, N. Poccia, A. Ricci, G. Campi, M. Burghammer, G. Aeppli, and A. Bianconi, Nature **466**, 841 (2010).
[27] A. Bianconi, D. Di Castro, S. Agrestini, G. Campi, N. L. Saini, A. Saccone, S. De Negri, and M. Giovannini, J. Phys.: Condens. Matter **13**, 7383 (2001).
[28] T. E. Weller, M. Ellerby, S. S. Saxena, R. P. Smith, and N. T. Skipper, Nat. Phys. **1**, 39 (2005).
[29] G. Csányi, P. B. Littlewood, A. H. Nevidomskyy, C. J. Pickard, and B. D. Simons, Nat. Phys. **1**, 42 (2005).
[30] K. Sugawara, T. Sato, and T. Takahashi, Nat. Phys. **5**, 40 (2009).
[31] A. Ricci, B. Joseph, N. Poccia, W. Xu, D. Chen, W. S. Chu, Z. Y. Wu, A. Marcelli, N. L. Saini, and A. Bianconi, Supercond. Sci. Technol. **23**, 052003 (2010).
[32] J. Paglione and R. L. Greene, Nat. Phys. **6**, 645 (2010).
[33] I. M. Lifshitz, Zh. Eksp. Teor. Fiz. **38**, 1569 (1960); Sov. Phys. JETP **11**, 1130 (1960).
[34] S. Agrestini, N. L. Saini, G. Bianconi, and A. Bianconi, J. Phys. A **36**, 9133 (2003).
[35] M. Fratini, N. Poccia, and A. Bianconi, J. Phys.: Conf. Ser. **108**, 012036 (2008).
[36] N. Poccia, A. Ricci, and A. Bianconi, Advances in Condensed Matter Physics **2010**, 261849 (2010).
[37] K. Ueno, S. Nakamura, H. Shimotani, A. Ohtomo, N. Kimura, T. Nojima, H. Aoki, Y. Iwasa, and M. Kawasaki, Nature Mater. **7**, 855 (2008).
[38] J. T. Ye, S. Inoue, K. Kobayashi, Y. Kasahara, H. T. Yuan, H. Shimotani, and Y. Iwasa, Nature Mater. **9**, 125 (2010).
[39] K. Prassides, Nature Mater. **9**, 96 (2010).
[40] X.-L. Qi, T. L. Hughes, S. Raghu, and S.-C. Zhang, Phys. Rev. Lett. **102**, 187001 (2009).
[41] E. M. Eagles, Phys. Rev. **186**, 456 (1969).
[42] A. Vittorini-Orgeas and A. Bianconi, J. Supercond. Novel Magn. **22**, 215 (2009).
[43] A. Perali, C. Grimaldi, and L. Pietronero, Phys. Rev. B **58**, 5736 (1998) and references therein.
[44] A. Bianconi, Solid State Commun. **91**, 1 (1994).
[45] N. Kristoffel, P. Konsin, and T. Ord, Riv. Nuovo Cimento **17**, 1 (1994).
[46] A. Bussmann-Holder, in *Superconductivity in Complex Systems*, edited by K. A. Muller and A. Bussmann-Holder, Structure and Bonding Vol. 114 (Springer, New York, 2005).
[47] E. J. Nicol and J. P. Carbotte, Phys. Rev. B **71**, 054501 (2005).
[48] C. T. Chen, C. C. Tsuei, M. B. Ketchen, Z. A. Ren, and Z. X. Zhao, Nat. Phys. **6**, 260 (2010).
[49] K. Kuroki, S. Onari, R. Arita, H. Usui, Y. Tanaka, H. Kontani, and H. Aoki, Phys. Rev. Lett. **101**, 087004 (2008).
[50] A. Perali, C. Castellani, C. Di Castro, M. Grilli, E. Piegari, and A. A. Varlamov, Phys. Rev. B **62**, R9295 (2000).
[51] P. Entel and D. Rainer, J. Low Temp. Phys. **23**, 511 (1976).
[52] A. Bianconi, D. Di Castro, S. Agrestini, G. Campi, and N. L. Saini, *Tc Amplification by Shape Resonance in MgB2, APS*, Seattle, March Meeting, 2001, MgB2 session, talk 72.
[53] A. Bianconi *et al.*, Phys. Rev. B **65**, 174515 (2002).
[54] O. de la Peña, A. Aguayo, and R. de Coss, Phys. Rev. B **66**, 012511 (2002).
[55] R. F. Klie, J. C. Zheng, Y. Zhu, A. J. Zambano, and L. D. Cooley, Phys. Rev. B **73**, 014513 (2006).
[56] S. Agrestini, C. Metallo, M. Filippi, L. Simonelli, G. Campi, C. Sanipoli, E. Liarokapis, S. Denegri, M. Giovannini, A. Saccone, A. Latini, and A. Bianconi, Phys. Rev. B **70**, 134514 (2004).
[57] O. De la Peña-Seaman, R. de Coss, R. Heid, and K.-P. Bohnen, Phys. Rev. B **79**, 134523 (2009).
[58] A. Bharathi, S. J. Balaselvi, S. Kalavathi, G. L. N. Reddy, V. S. Sastry, Y. H. Hariharan, and T. S. Radhakrishnan, Physica C **370**, 211 (2002); S. Lee, T. Masuia, A. Yamamoto, H. Uchiyama, and S. Tajima, *ibid.* **397**, 7 (2003).
[59] D. Daghero, R. S. Gonnelli, A. Calzolari, G. A. Ummarino, V. Dellarocca, V. A. Stepanov, N. Zhigadlo, S. M. Kazakov, and J. Karpinski, Phys. Status Solidi C **2**, 1656 (2005).
[60] P. Samuely, P. Szabo, P. C. Canfield, and S. L. Bud'ko, Phys. Rev. Lett. **95**, 099701 (2005).
[61] P. Samuely, Z. Holanova, P. Szabo, H. T. Wilke, S. L. Bud'ko, and P. C. Canfield, Phys. Status Solidi C **2**, 1743 (2005).
[62] L. D. Cooley, A. J. Zambano, A. R. Moodenbaugh, R. F. Klie, Jin-Cheng Zheng, and Yimei Zhu, Phys. Rev. Lett. **95**, 267002 (2005).
[63] M. Putti, C. Ferdeghini, M. Monni, I. Pallecchi, C. Tarantini, P. Manfrinetti, A. Palenzona, D. Daghero, R. S. Gonnelli, and V. A. Stepanov, Phys. Rev. B **71**, 144505 (2005).
[64] S. Tsuda *et al.*, Phys. Rev. B **72**, 064527 (2005).

[65] H. Olijnyk, A. P. Jephcoat, D. L. Novikov, and N. E. Christensen, Phys. Rev. B **62**, 5508 (2000).
[66] A. F. Goncharov and V. V. Struzhkin, Physica C **385**, 117 (2003).
[67] L. Simonelli, V. Palmisano, M. Fratini, M. Filippi, P. Parisiades, D. Lampakis, E. Liarokapis, and A. Bianconi, Phys. Rev. B **80**, 014520 (2009).
[68] H. J. Choi, D. Roundy, H. Sun, M. L. Cohen, and S. G. Louie, Phys. Rev. B **66**, 020513 (2002).
[69] H. J. Choi, D. Roundy, H. S. M. L. Cohen, and S. G. Louie, Nature (London) **418**, 758 (2002).
[70] G. A. Ummarino, R. S. Gonnelli, S. Massidda, and A. Bianconi, Physica C **407**, 121 (2004).
[71] A. Bussmann-Holder and A. Bianconi, Phys. Rev. B **67**, 132509 (2003).
[72] Yu. E. Lozovik and A. A. Sokolik, Phys. Lett. A **374**, 326 (2009).